Available online at www.sciencedirect.com
ScienceDirect
Journal of Nuclear Materials 375 (2008) 86–94
journal of nuclear materials
www.elsevier.com/locate/jnucmat

Characterization of plutonium distribution in MIMAS MOX by image analysis

Ghislain Oudinet [a], Isabelle Munoz-Viallard [a], Laurence Aufore [a,*], Marie-Jeanne Gotta [a], J.M. Becker [b], G. Chiarelli [c], R. Castelli [c]

[a] *Commissariat à l'Énergie Atomique (CEA), Département d'Étude des Combustibles – CEA/Cadarache, F-13108 Saint-Paul-Lez-Durance, France*
[b] *CPE (Chimie Physique Électronique) Lyon Bat. 308, 43 bd du 11 novembre 1918, F-69616 Villeurbanne cedex, France*
[c] *COGEMA, Business Unit Recycling – 30204 Bagnols sur Cèze cedex, France*

Received 21 July 2006; accepted 31 October 2007

Abstract

A better understanding of MOX fuel in-pile behaviour requires a very detailed characterization of the Pu distribution in the pellet before and after irradiation. Electron probe microanalysis (EPMA) can be used to determine the distributions of chemical elements with a spatial resolution of 1 μm. This paper describes the development of X-ray microanalysis techniques to produce semi-quantitative 'maps' of plutonium concentrations in order to rapidly characterize large areas of the fuel microstructure (1 mm^2) with reasonable accuracy. A new segmentation technique based on statistical compatibility is then proposed, so as to finely describe the MIMAS MOX fuel microstructure. Two materials were finely characterized to demonstrate the reliability of this new method. In each case, the results demonstrate the good and reliable accuracy of this new characterization methodology. The analysis method used is currently able to identify three so-called phases (Pu-rich agglomerates, a coating phase and uranium-rich agglomerates), as well as to quantify the plutonium distribution and the plutonium content of these three phases. The impact of the fabrication process on the microstructure can be seen both in the surface distribution variations of the plutonium and in the local plutonium content variations.

1. Introduction

MOX fuel has been used in French PWRs since 1987. In October 2005, about 2400 MOX fuel assemblies (1100 tM of MOX) had been loaded in 20 different EDF 900 MWe reactors. Maximum MOX assembly burn-up is currently 42 GWd/tM, but several experimental rods have reached a burn-up close to 60 GWd/tM.

As UO_2 fuel is allowed to operate up to 52 GWd/tM, this burn-up stands as the first objective for MOX fuel in order to reach what is called 'MOX parity' (same management and burn-up for UO_2 and MOX), which has been planned to start in 2007 [1]. Increasing the performance of MOX fuels relies on knowledge and understanding of the in-pile behaviour of the current MOX fuel. Irradiated fuel surveillance programs conducted since the beginning of plutonium recycling in French PWRs have shown that fission gas releases are higher in MOX fuel rods than in UO_2 fuel rods at the same burn-up [2–4].

These higher gas releases in MOX fuels can be clearly explained by two reasons and possibly a third one:

- for reasons owing to core physics, the power density – and hence the linear heat rate – decreases at a slower rate in MOX fuels than in UO_2 fuels,
- the thermal conductivity of MOX fuel is slightly lower than that of UO_2: the centerline temperature is therefore higher, even at the same power [5],
- the microstructure of the MOX pellets exhibits a non homogeneous distribution of plutonium. These pellets were fabricated by the MIMAS (MIcronized MASter blend) process in which a primary blend of UO_2 and

* Corresponding author. Fax: +33 4 42 25 47 17.
E-mail address: laurence.aufore@cea.fr (L. Aufore).

0022-3115/$ - see front matter © 2007 Elsevier B.V. All rights reserved.
doi:10.1016/j.jnucmat.2007.10.013

PuO_2 is diluted with UO_2. Is this special microstructure partly responsible for higher gas releases? Some studies have shown differences in gas releases for MOX fuels elaborated with different manufacturing processes and/or different UO_2 [6,7].

Thanks to a detailed investigation of the evolution in the fuel microstructure and the fission gas behaviour, it is now possible to draw a more comprehensive picture of the mechanisms related to gas releases and of the influence of the initial microstructure on these mechanisms. Fission gas release models and codes developed by the CEA [8] are able to integrate the MOX microstructure effect in order to improve the modelling of the in-pile behaviour of MOX fuel. These models use the characterizations of as-fabricated MOX fuel as input data and are used to validate the characterization of irradiated MOX.

This paper explains the methods developed to characterize initial MOX fuel microstructures – especially the plutonium distribution within the fuel – using microprobe images. This point is very important because the local fission density is directly related to the way fissile plutonium atoms are initially distributed in the material.

This paper first describes the automated method of semi-quantification of X-ray maps associated with the plutonium element. The paper then describes the method of automatic segmentation into several compounds (typical of MOX fuel) based on the counting statistic associated with this image acquisition technique. All these methods are then applied to two different industrial fuels.

2. Presentation of the analyzed material

The MIMAS (MIcronized MASter blend) process is today the most widely used industrial process for MOX fuel. It consists of two distinct steps. A mixed powder made up of plutonium dioxide, uranium dioxide and scrap with a total plutonium content lower than 30% is finely ground. The obtained powder, called 'master blend', is then sifted and diluted in uranium dioxide to reach the desired plutonium content. This secondary mixture is pressed into pellets, which are then sintered and centerless ground to the specified diameter.

Uranium oxide and plutonium oxide can form solid solutions $(U,Pu)O_2$, but the apparent interdiffusion coefficients of U and Pu are very slow under reducing conditions ($\widetilde{D}_{bulk} \approx 2.10^{-14}\ m^2/s$ at 2000 K and $\Delta G_{O_2} = -380$ kJ/mole) [9]. Manufacturing sintering conditions are unfavourable for both homogenisation and the formation of solid solutions of UO_2–PuO_2 mixtures.

The manufacturing process results in a material consisting of plutonium-free U-rich agglomerates and Pu-rich agglomerates with a plutonium content close to that of the master blend. These agglomerates are separated by a coating phase whose plutonium content is between 0 and that of the master blend. Hereafter, the term 'phase' will be used to distinguish fractions of the material with the different plutonium concentrations, and not in the sense usually intended in thermodynamics.

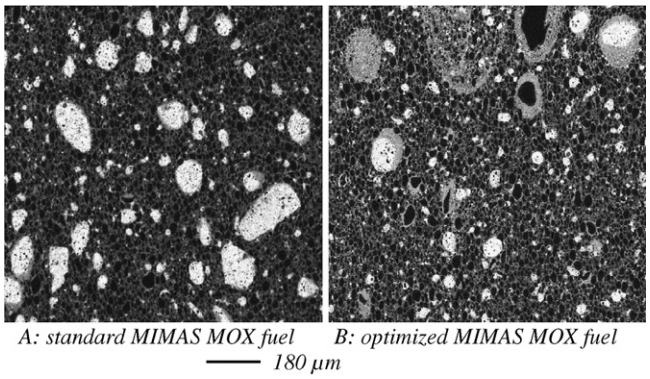

Fig. 1. X-ray images of Pu in non-irradiated standard MOX (materials A and B).

The studied materials A and B are industrial fuels manufactured by COGEMA – MELOX

- A is a typical standard MOX MIMAS; it is a pellet with a high plutonium content (7.2% Pu/(U + Pu)) randomly sampled from of a MELOX batch.
- B is an experimental MOX MIMAS fuel with a high plutonium content (7.1% Pu/(U + Pu)) processed so that the plutonium agglomerates are smaller than the standard ones [10,11].

On the microscopic scale, the X-ray maps acquired with an electronic microprobe allow the fine analysis of the coating phase in which UO_2 and PuO_2 form a continuous solid solution (Fig. 1, where darker pixels correspond to low plutonium concentration).

A universal characterization method for this step is required to objectively compare the different batches and to quantify the evolution of their microstructure during irradiation.

First, Garcia et al. [12] analyzed the microstructure using microprobe examinations of MOX MIMAS fuels manufactured by Belgonucléaire. X-ray maps were analysed using the common method of histogram thresholding. The threshold was defined as the grey level at which the second derivative of the greyscale histogram reaches a local maximum. Our aim was to look for a more robust method that was not too sensitive to the operator effect and to the image noise.

Image analysis is an efficient tool used to develop automated methods of semi-quantification and segmentation for microprobe maps [13,14]. These methods are described below.

3. Experimental methods

The experimental method was performed in three stages:

- acquisition of X-ray mapping of plutonium,
- quantification of the image,
- segmentation of the image.

The originality of this study is based upon the technique of semi-quantification of the image and the method of segmentation using a semi-quantified image.

3.1. Microprobe image acquisition

The number of X-ray maps to be acquired depends on the homogeneity on the manufacturing batch. Within the framework of this study, a longitudinal section and a cross section were produced. On each metallographic cut, three fields (1024×1024 pixels; 1 mm^2) were randomly selected using the displacement mode of the sample holder stage. Measurements were carried out on the Pu, U and O peaks without subtracting the background noise of the spectrum (continuous background). The select counting time was almost 20 ms per pixel, which represented approximately 6 h of data acquisition per field (the sample holder moves, as the X-ray beam is fixed). The image remains stable.

3.2. Method of semi-quantification

3.2.1. Acquisition of a quantitative line

Each X-ray map is connected to a quantitative profile taken randomly on the image. Such profiles are acquired by steps of 1 μm in size. Intensities measured on the Mβ line of Pu of both the standard and the samples to be analyzed are corrected taking into account the background noise and removing the interference between the plutonium Mβ line and the uranium Mγ line. An accurate plutonium concentration is then measured based on the relative intensity between the analyzed sample and the standard by means of ZAF-type correction factors. The counting duration over each point lasts 15 s for peaks and 10 s for the continuous background. The standards used are pure UO_2 for uranium and oxygen, and pure PuO_2 for plutonium. The acceleration voltage of electrons and the intensity of the probe current selected for the quantitative analysis are respectively equal to 20 kV and 80 nA.

3.2.2. Calibration line

By associating a qualitative X-ray map of Pu with a quantitative profile, it is possible to establish a calibration line giving the Pu content versus counts per nA and per sec (grey level) acquired for each pixel of the image. With this objective in mind, the first stage consists in extracting the grey level profile corresponding exactly to the quantitative profile analyzed on the image. However, precise positioning on X-ray maps of the points of the profile to be quantified (materialized by the pixels of the image) depends on the accuracy of the displacement of the sample holder stage, as well as on slight fluctuations in the acquisition conditions. Thus, an algorithm of correlation is used to precisely locate this profile on the image (Fig. 2). The coefficients of correlation obtained are greater than 0.95. A set of qualitative profiles which cross the same phases in other directions is chosen. Each such profile can be stretched and shifted upward or downward to fit the quantitative profile. For a given Pu concentration the corresponding grey levels in each qualitative profile are averaged. The averaging method which leads to an equation translating grey levels of the image into plutonium concentrations can then be established by means of a linear weighted least squares regression such as those described in details by Ancey et al. [15]. The qualitative greyscale image is transformed into a semi-quantified image.

3.3. Segmentation method

Traditional methods of thresholding grey level histograms (maximization of the variance between classes [16],

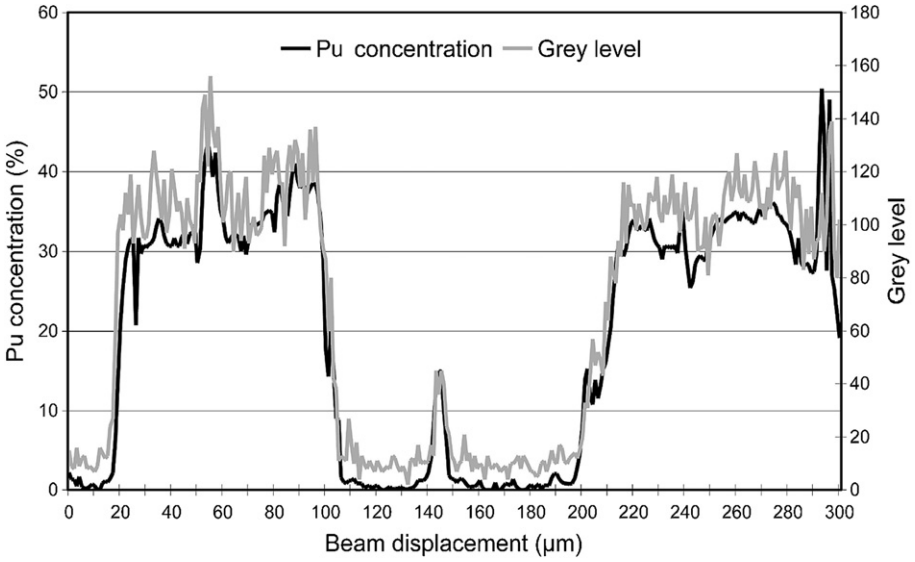

Fig. 2. Agreement between a quantitative profile and grey levels of pixels extracted from an electronic microprobe image (laboratory sample).

maximization of entropy [17,18], methods using various order derivatives of the histogram [19], etc.) proved to be rather unreliable and too sensitive to the image background noise. Considering the quality of the images (with more or less noise) and the specificity of our material (continuous solid $(U,Pu)O_2$ solution of varying Pu compositions), we chose to use a method based on both the 2D location of the image points and their plutonium concentration, in order to segment the agglomerates in one step only and not successively as it is the case for segmentation and morphology remodelling techniques. The specific method of thresholding proposed within the framework of this study simultaneously integrates grey levels and the vicinity of each pixel. In addition, it takes into account the counting statistics associated with X-ray emissions making it possible to determine a confidence interval for each mean measured value. Counting associated with each measurement point follows a Poisson-type statistical distribution. Consequently, starting from the semi-quantified image, zones statistically compatible with the initial content of the master blend (representing plutonium rich agglomerates) can be defined, as can be those compatible with null plutonium content (representing uranium agglomerates). Remaining zones are subjected to a more complex analysis, with their plutonium content being between that of plutonium rich zones and that of uranium-rich ones.

The geodesic distance to the nearest plutonium agglomerate is associated with each point of the image. This distance is equal to the length of the shortest path connecting this point to a plutonium agglomerate, thus circumventing uranium agglomerates. X-ray maps are then transformed into a geodesic chart of distances, where the level of grey of each point not belonging to a plutonium agglomerate is proportional to the shortest distance separating it from a plutonium agglomerate. This chart enables us to study the average plutonium concentration as a function of the distance to the nearest plutonium-bearing cluster. The layout of the graph (see Fig. 3) – representing the average plutonium concentration of a point on the image according to its distance to the nearest plutonium agglomerate (among two studied fuels) – is the cornerstone of the method of segmentation recommended hereafter.

This graph highlights a major reduction in the plutonium concentration within the first micrometers surrounding clusters and a stabilization at long distances. Fluctuations at the end of the graph come from a low statistical representativeness (few points of the image are located so far from plutonium agglomerates). The decrease in plutonium and the stabilization of the plutonium content showed two definitely linear profiles. The graph can thus be modelled by two segments: one directed almost vertically, the other directed almost horizontally.

The maximum concentration – obtained at zero distance from the plutonium agglomerates – is characteristic of the minimal content in the agglomerate cores. The right-hand side of the graph (approaching the horizontal one) is considered characteristic of the average content of the coating phase. The level of thresholding in concentration is thus to be located between the low limit associated with the master blend, and the mean level of concentration associated with the coating phase (intersection between the two segments). Agglomerate boundary is relatively well-defined (Fig. 2), so we chose to use empirical thresholding, to compare the different manufacturing batches. The level of thresholding could be chosen halfway between these two levels of concentration or nearer to the Pu agglomerate (threshold used for this study) or nearer to the coating phase (see Fig. 3). Uranium agglomerates cannot be subjected to the same treatment insofar as their grey levels include a considerable amount of background noise. Thus, they are simply assimilated to their core on the grounds of statistical compatibility. Based on conventional statistical methods, for a grey level n associated with a given plutonium concentration,

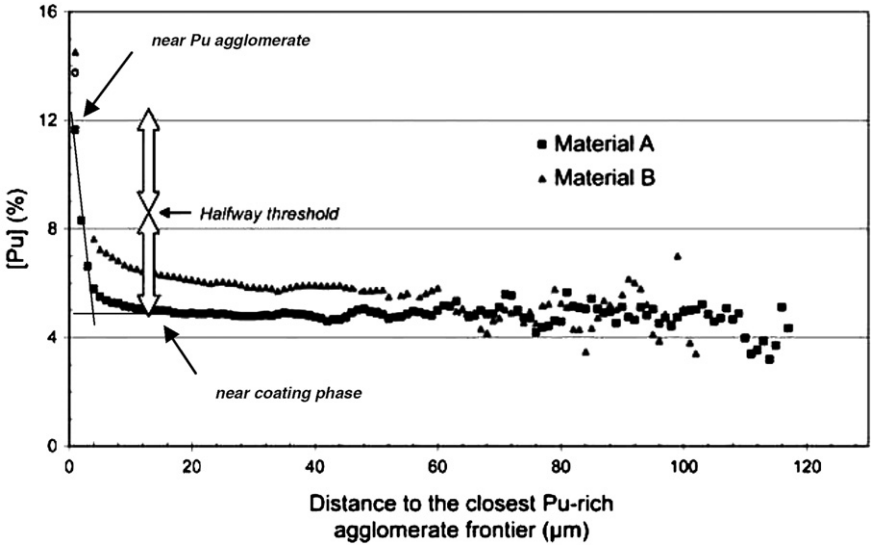

Fig. 3. Mean Pu concentration versus the distance to the closest Pu-rich agglomerate.

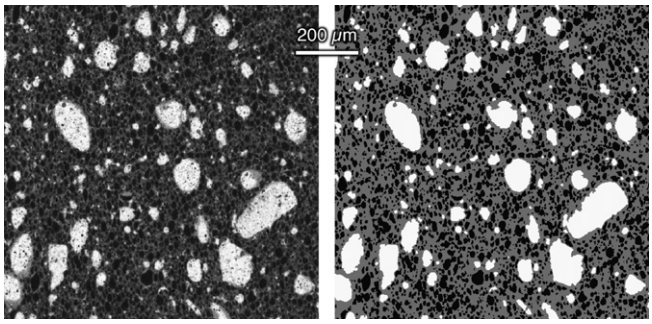

Fig. 4. Segmentation result (material A).

the levels of grey ranging between $n-2\sqrt{n}$ and $n+2\sqrt{n}$ are considered compatible with n. Fig. 4 illustrates the segmentation of the image illustrated in Fig. 1 for sample A. The three phases are clearly identified. The morphology of the uranium agglomerates (black zones) and the plutonium agglomerates (white zones) is respected. The coating phase (grey zone) appears to be connected, which is coherent from a physical point of view.

The interest of this method is primarily based on consideration of the vicinity of each pixel on the image, making it possible to dissociate the pixels belonging to the master blend of a local over-concentration of fine plutonium particles on the one hand, and to adapt to any type of agglomerate morphology on the other hand.

3.4. Qualification of the data processing method

Our quantification method was qualified by comparing the results obtained during precise quantitative measurements using a microprobe on a 2500 points grid (20 s of acquisition time with a current of 76 nA), with those obtained in the same field using the microprobe qualitative image and our translating equation from grey levels to concentrations. The results obtained on part of a U-rich agglomerate and part of a Pu-rich agglomerate (Table 1) show the plutonium quantification results of part of a microprobe image belonging to a MOX fuel.

NB: This qualification is based on sample other than A and B. More specifically, the initial plutonium concentration of the master blend in this sample is 36%.

Taking into account systematic errors due to: sample preparation (polishing, impurities, roughness), instrumental parameters (spectrometer efficiency, position, intensity...), quantification calculations (ZAF corrections), the evaluation of the global uncertainty can deviate by about 10% absolute, but the relative error is lower than 2%.

4. Experimental results on fresh fuel

4.1. Detection of phases

The result of the phase segmentation differentiates three phases within the MOX MIMAS fuel and determines the surface fraction of each of them. The surface fraction of the phases is shown in Table 2 for the analyzed materials. The uncertainties associated with the calculated values correspond to the scatter among the six analyzed fields per batch (confidence interval with two times the standard deviation). These uncertainties are comparable from one batch to another. The volume percentage of the master blend introduced during the fabrication phase is close to 26%. The proportionality factor between the amount of master blend introduced during fabrication and the surface fraction of agglomerates measured by image analysis is noted Fp. This factor is greater than 1 since a noticeable part of the plutonium is transferred in the coating phase during the subsequent fabrication steps. It is close to 2 in the case of batch A and greater than 3 in the case of batch B (Table 2). The difference noticed in the Fp factor shows the influence of the grinding–sifting process. The plutonium and uranium phases are less extensive in batch B where the coating phase is predominant. This is illustrated in the microprobe image shown in Fig. 1, sample B.

Table 1
Qualification of the quantification method (laboratory sample)

Pu (%)	Pu-rich agglomerate	U-rich agglomerate
Quantitative map	36.09 ± 0.01[a]	0.19 ± 0.01[a]
Calibrated qualitative map	36.2 ± 0.2[b]	0.00 ± 0.12[b]

[a] Standard deviation provided by measuring the scattering of the 2500 analysed points (quantitative measurements).
[b] Uncertainty provided by subtracting results obtained from the calibrated qualitative map to the quantitative map.

4.2. Size spectrum of Pu-rich agglomerates

Within the framework of the R&D program on MOX fuels, the aim was to reduce the size of the plutonium-enriched agglomerates [12]. This parameter may influence the retention and/or release of fission gases especially during in-pile irradiation, although this effect has not yet been fully quantified [6,7]. The comparison between batches A and B showed that with a similar final Pu content, the size spectrum of the Pu-rich agglomerates has changed towards smaller sizes. One can notice on the cumulated graph that in batch B, more plutonium is contained into small size agglomerates, which was the expected goal (Fig. 5). In batch B, cumulated plutonium percentage is about 29% of the total plutonium content, in the Pu-rich agglomerate, to be compared to 42% in the case of batch A.

Table 2
Phases distribution (including scattering uncertainty) and proportionality factor Fp

	Material A	Material B
Pu-rich agglomerate (area %)	14 ± 2	7 ± 1
'Coating phase' (area %)	51 ± 1	61 ± 1
U-rich agglomerate (area %)	36 ± 1	31 ± 1
Fp	1.9	3.5
Total Pu content (%)	7.2	7.1

4.3. Size spectrum of U-rich agglomerates

The size spectrum of uranium agglomerates is illustrated in Fig. 6. The granulometric distribution of the initial UO_2 rough powder batches is currently about 30 μm. This spectrum tends to move towards slightly smaller sizes owing to (a) the sintering shrinkage (about 15% of the volume), (b) the small U/Pu global interdiffusion, and (c) a possible erosion of the agglomerates during the dilution phase in the fabrication process. Fig. 6 shows distributions centred on 20 μm. The average calculated sizes for the U-rich agglomerates are 27 μm and 20 μm, respectively.

4.4. Total plutonium content

The quantification of the microprobe images makes it possible to determine both the average plutonium content of the analyzed fields and the average plutonium content of each phase. Table 3 illustrates the differences observed between the calculated values and the experimental values measured by the chemical dissolution of $(U,Pu)O_2$ pellets. Good agreement is obtained between the calculated values using the quantification method and those expected, according to the chemical dissolutions.

4.5. Analysis of different phases: quantification of their distribution and plutonium concentration

The surface distribution is analyzed as a function of the three phases: plutonium rich agglomerates, coating phase and uranium agglomerates. An element of comparison was defined by the Fp factor. For the same fabrication process, this factor may take different values (Table 2). This indicates that the final content in the Pu-rich agglomerates is not directly proportional to the volume fraction of master blend introduced.

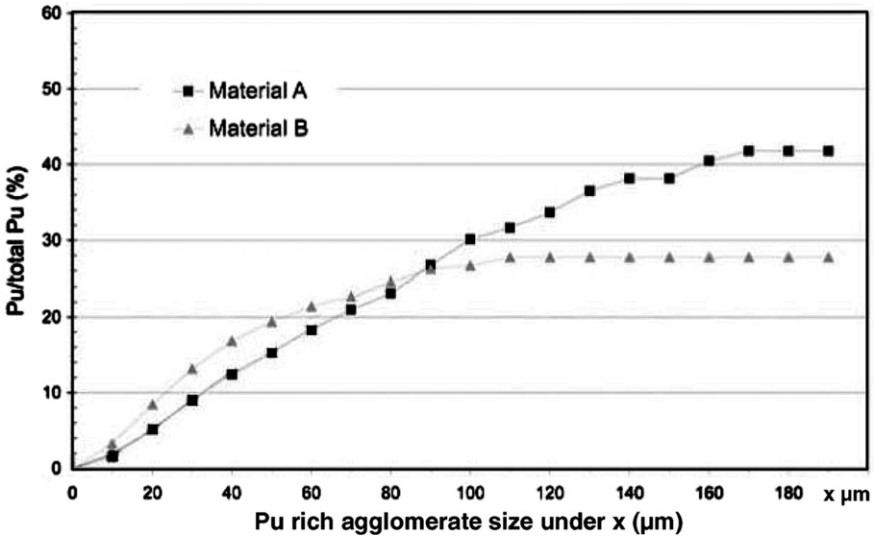

Fig. 5. Pu-rich agglomerate size spectra and cumulated plutonium percentage relative to the total plutonium content.

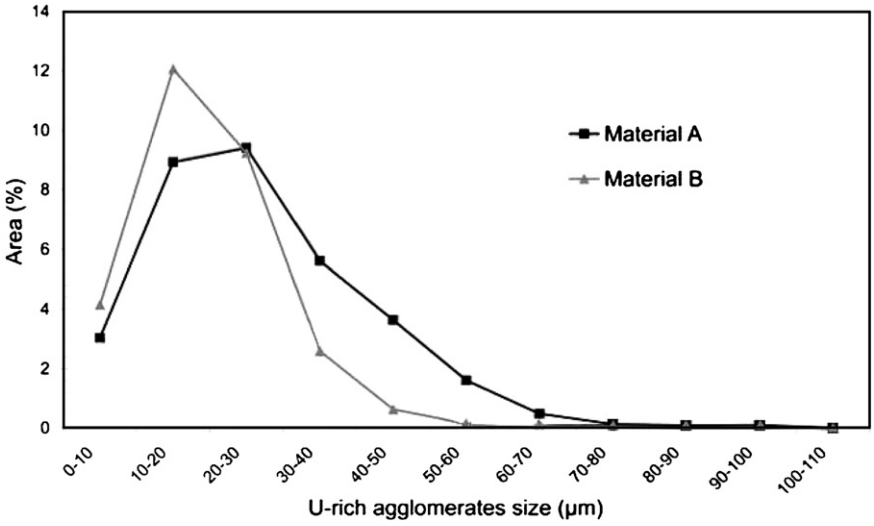

Fig. 6. U-rich agglomerate size spectra.

Table 3
Total Pu content

Pu/(U + Pu) content (wt%)	Material A	Material B
Calculated	7.2 ± 0.4	7.4 ± 0.3
Experimental	7.2	7.1

Table 4
Phases Pu content

Pu content (wt%)	Material A	Material B
Pu-rich agglomerate	24.0 ± 0.2	23.9 ± 0.2
'Coating phase'	5.7 ± 0.1	7.1 ± 0.2
U-rich agglomerate	0.5 ± 0.1	0.5 ± 0.1

Table 5
Pu distribution inside the phases of the two tested materials

Pu/Pu total%	Material A	Material B
Pu-rich agglomerate	51 ± 4	30 ± 2
'Coating phase'	46 ± 3	67 ± 2
U-rich agglomerate	3 ± 1	3 ± 1

For the batch B, the percentage of Pu-rich agglomerates is reduced and the fine particles are spread into the 'coating phase', which then becomes the largest phase. The quantity of agglomerates coming from the master blend and their morphological characteristics (cohesion degree, granulometry, density, etc.) both have a direct impact on the plutonium distribution in the final sintered pellet.

The mean plutonium content in each of the phases has been quantified (Table 4). Both batches have master blend agglomerates with an equivalent plutonium content (about 24% Pu/(U + Pu)O_2).

It is worth noting that for batch B, much more than half of the plutonium is contained in the coating phase (67 % total Pu) (Table 5). In a standard MOX fuel, the plutonium is equally divided between the two phases: agglomerates and coating. The microprobe coupled with the image analysis treatment provided a better understanding of the microstructure of MOX fuels on a microscopic scale.

5. Segmentation method on a two-cycle irradiated fuel

5.1. Segmentation

The irradiation of fuel in a reactor has two main consequences:

- the plutonium is burned by fission reactions that locally reduce its concentration and add much lighter fission products,
- the neutronic fertilization of ^{238}U increases the plutonium content in the uranium zones.

Within a fuel pellet, the progressive averaging of the plutonium concentration during irradiation makes it more difficult to identify plutonium areas. It is however of major importance to be able to analyze fresh fuel and irradiated fuel in the same way so as to characterize the fuel's evolution.

As the above-mentioned segmentation method is based on the notion of homogeneous domain, we decided to test it on fuel that had been irradiated for two-cycles.

5.2. Experimental results

The analyzed material was a two-cycle irradiated MOX MIMAS fuel. The average pellet content (4.86% Pu/(U + Pu)) was determined by microprobe analysis. We created a 126-point quantitative profile (1 μm^2 per point) and a qualitative map (area of 1024 × 1024 pixels with 1 μm^2 per pixel and grey levels ranging from 1 to 199).

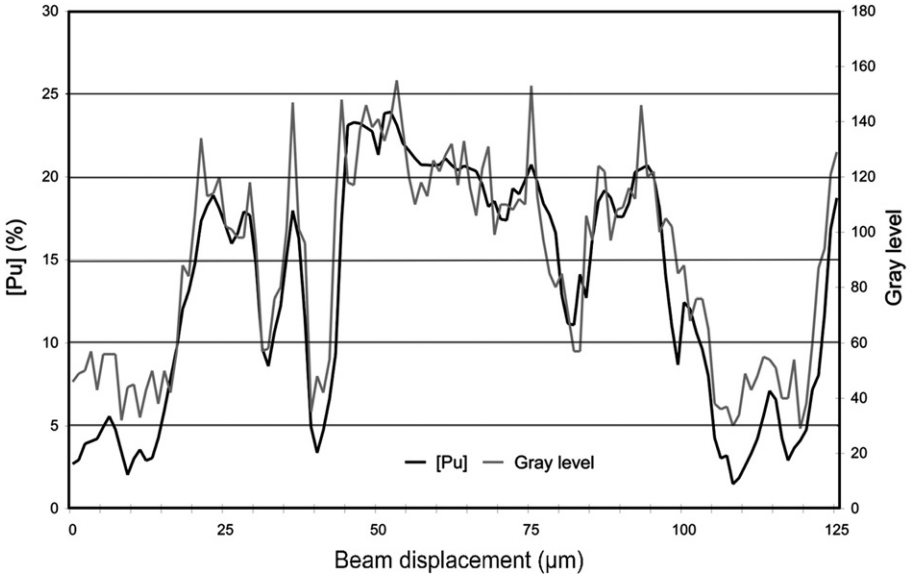

Fig. 7. Agreement between the Pu concentration and the grey levels on an image of a two-cycles irradiated fuel.

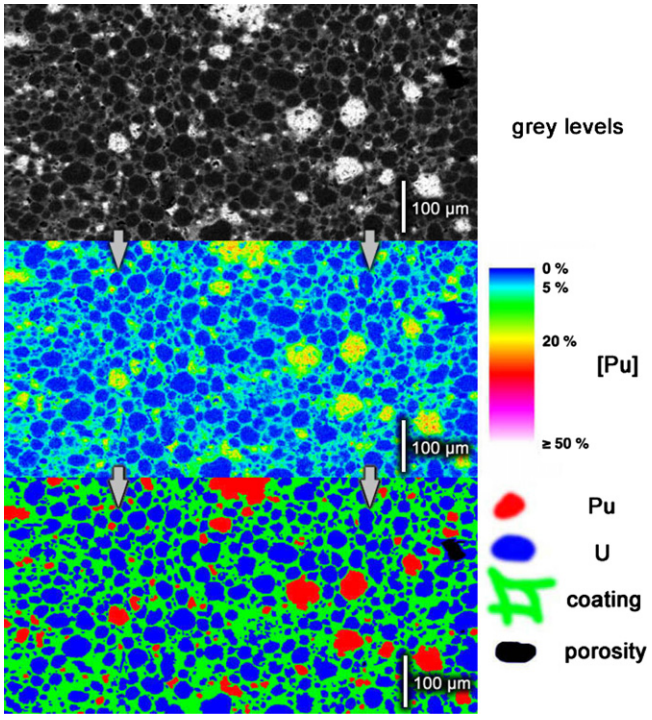

Fig. 8. Application of the segmentation method to an image of a two-cycle irradiated fuel.

The semi-quantification of the image of the material led to a positioning of the profile on the map with a correlation coefficient of 0.93 (Fig. 7). The average calculated value of the field is then 4.62% Pu/(U + Pu), which is consistent with the field scattering (a few tenths of percent).

Our segmentation method is based on the knowledge of the plutonium content in the 'core' of the agglomerates, as well as nil content in plutonium in the 'core' of uranium agglomerates. These assumptions are not verified in the case of irradiated fuel. This is why the plutonium content in the 'cores' of the different agglomerates (Pu-rich, and U-rich) was evaluated using recordings from the semi-quantified map.

Following the semi-quantification and segmentation phases, the agglomerates and the coating phase are correctly detected (qualitative examination) and in a similar way to what is obtained on fresh fuel (Fig. 8).

The segmentation method will require more validation tests on irradiated fuel. However, its operating principle and preliminary results indicate that the characterization of two-cycle irradiated fuels is of equivalent quality to that obtained for fresh fuel. The lack of matter (pores, cracks) that appears during irradiation is easily identifiable, which is of considerable interest when aiming to accurately characterize irradiated fuels.

6. Conclusion

The industrial objective of increasing the burn-up of MOX fuels in France to 52 GWd/tM and then beyond this value requires further analysis and understanding of the behaviour of MOX fuel under irradiation. It is thus necessary to set up and qualify tools designed to provide an in-depth characterization of microstructures. By developing and validating a method – on both fresh and irradiated fuel – that is based on an automatic threshold of images acquired with a Castaing electronic microprobe, it is possible to quantify the different phases (UO_2, Pu-rich agglomerates and coating phase) and improve comparison between the different types of MOX microstructures. Quantified elements are given for the distribution and the plutonium content of the three detected phases. This shows that the fabrication process has a noticeable impact on the phase distribution. The objective to obtain a more homogeneous Pu distribution with Pu-rich agglomerates of reduced size has therefore been reached.

References

[1] J.L. Provost, M. Debes, MOX and UOX PWR Fuel Performances – EDF Operating Experience, Water Reactor Fuel Performance Meeting, Kyoto, October 2005.
[2] L. Brunel, P. Blanpain, G. Chaigne, M. Trotabas, in: International Symposium on MOX Fuel Cycle Technologies for Medium and Long Term Deployment, Vienna, Austria, May, 1999.
[3] P. Blanpain, X. Thibault, M. Trotabas, in: ANS International Topical Meeting on Light Water Reactor Fuel Performance, West Palm Beach, April 1994.
[4] P. Blanpain, X. Thibault, P.J. Pagès, in: ANS International Topical Meeting on Light Water Reactor Fuel Performance, Portland, Oregon, March 1997.
[5] L. Caillot, G. Delette, J.P. Piron, C. Lemaignan, A. Chotard, J.P. Berton, in: ANS International Topical Meeting on Light Water Reactor Fuel Performance, Portland, Oregon, March 1997.
[6] Y. Guerin, J. Noirot, D. Lespiaux, C. Struzik, P. Garcia, P. Blanpain, G. Chaigne, in: Proceeding of the International Topical Meeting on Light Reactor Performances, Park City, USA, April 2000.
[7] S.B. Fischer, R.J. White, P.M.A. Cook, S. Bremier, R.C. Corcoran, R. Stratton, C.T. Walker, P.K. Ivison, I.D. Palmer, J. Nucl. Mat. 306 (2002) 153.
[8] C. Struzik, M. Moyne, J.P. Piron, in: ANS International Topical Meeting on Light Water Reactor Fuel Performance, Portland, Oregon, March 1997.
[9] S. Pillon, S. Mendez, D. Warin, R. Lorenzelli, in: Proceedings of the AIEA Technical Committee Meeting on Recycling of Plutonium and Uranium in Water Reactor Fuel, 3–7 July 1995, Newby Bridge, UK, IAEA-TECDOC-941.
[10] P. Blanpain, C. Callens, W. Goll, G. Chiarelli, J.L. Guillet, in: TOP FUEL, Stockholm, May 2001.
[11] C. Delafoy, P. Blanpain, S. Lansiart, Ph Dehaudt, G. Chiarelli, in: AIEA Technical Meeting on Improved Fuel Pellet Materials and Design, Brussels, Belgium, 20–24 October 2003.
[12] P. Garcia, A. Bouloré, Y. Guérin, M. Trotabas, P. Goeriot, in: Proceeding of the International Topical Meeting on Light Reactor Performances, Park City, USA, April 2000.
[13] G. Oudinet, I. Munoz-Viallard, M.J. Gotta, J.M. Becker, G. Chiarelli, R. Castelli, in: AIEA Technical Meeting on Improved Fuel Pellet Materials and Design, Brussels, Belgium, 20–24 October 2003.
[14] G. Oudinet, Analyse d'images et modélisation 2D/3D de la microstructure du combustible MOX, Thèse de l'Université Jean Monnet, Saint-Étienne, March 2003.
[15] M. Ancey, F. Bastenaire, R. Tixier, J. Phys. D 10 (1977) 817.
[16] M. Coster, J.L. Chermant, Précis d'analyse d'images, Presse du CNRS, 1989, March.

[17] J.N. Kapur, P.K. Sahoo, A.K.C. Wong, Comput. Vision Graph. Image Process. 29 (1985) 273.
[18] R. Zeboudj, Filtrage, seuillage automatique, contraste et contours: du prétraitement à l'analyse d'images, Thèse de l'université de Saint-Etienne, April 1988.
[19] P. Garcia, A. Bouloré, Y. Guérin, M. Trotabas, Ph. Goeriot, In Pile Densification of MOX Fuels in Relation to their Initial Microstructure, American Nuclear Society, Annual Meeting Park City, April 2000.